ACS OMEGA

Open Access

http://pubs.acs.org/journal/acsodf

Article

Mechanism and Process Optimization in the Electrooxidation of Oxalic Acid Using BDD Electrode under Nitric Acid Environment

Lu Qiao, Hu Zhang,* Jing Zhao, Zhijun Cen, and Ting Yu

Cite This: *ACS Omega* 2024, 9, 49839−49848

Read Online

ACCESS | Metrics & More | Article Recommendations

ABSTRACT: Various electrochemical tests were carried out to elucidate the electrolytic oxidation mechanism of oxalic acid on a boron-doped diamond electrode in a nitric acid environment. These included cyclic voltammetry, AC impedance, constant current electrolysis, and electron paramagnetic resonance spectroscopy. The impact of electrode potential, current density, nitric acid concentration, and electrode plate spacing on the oxidation of oxalic acid was investigated. In the electrolysis mechanism, indirect oxidation of •OH plays a major role and direct oxidation at the electrode plays a minor role. Excessive nitric acid concentration will reduce the electrooxidation rate of oxalic acid. The optimal process conditions for electrolyzing oxalic acid are obtained as follows: the plate spacing is 2 cm, and the current density is 60 mA cm^{-2}. Finally, the BDD electrode can electrolyze the oxalic acid concentration to below 0.001 mol/L, which can meet the process requirements.

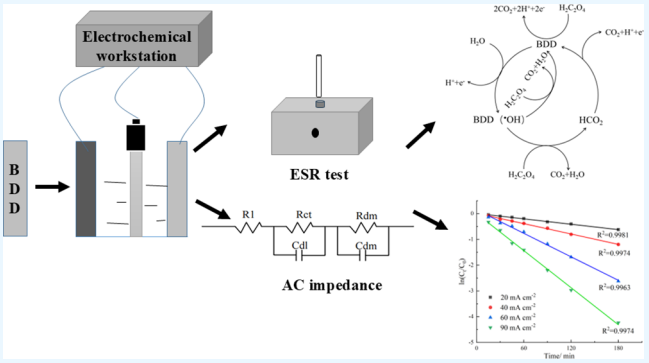

1. INTRODUCTION

During the nuclear fuel reprocessing process, oxalic acid in the plutonium oxalate mother liquor still retains trace amounts of plutonium and oxalic acid. The potent chelating capability of oxalic acid toward plutonium consequently impacts the recovery rate of plutonium in the purification cycle. Hence, the degradation of oxalic acid becomes crucial for achieving an effective purification cycle for plutonium.

In the exploration of oxalic acid degradation, various methods are employed, such as direct chemical reagent destruction,[1] photochemical degradation,[2] hydrogen peroxide oxidation,[3] electrochemical destruction,[4] etc. The electrochemical oxidation of oxalic acid exhibits a rapid decomposition rate, minimal waste generation, safe operation, and thorough destruction. The boron-doped diamond (BDD) electrode is gaining increasing attention for its ability to generate hydroxyl radicals easily, resistance to surface adsorption, wide electrochemical window, and corrosion resistance.[5] This electrode yielded promising results across various wastewater treatment applications. Hence, it can significantly contribute to the post-treatment of oxalic acid in the mother liquid. The remarkable oxidation capability of the BDD electrode relies on hydroxyl radicals, the second strongest oxidant known after fluorine, possessing an exceptionally high standard reduction potential. This property enables the rapid degradation of organic matter. The hydroxyl radical has emerged as a noteworthy player in the degradation of toxic pollutants, owing to its potent oxidizing capabilities and nontoxic properties. Hydroxyl radical (•OH) is characterized as "short-lived and difficult to capture," and there are two main methods for the detection of •OH. The first is to use electron spin resonance spectroscopy (ESR) in the presence of a spin trap, which is a compound that can selectively react with free radicals to form adduct species that have a lifetime long enough to be detected by ESR. The second approach uses probe compounds that react selectively with •OH and often form adducts that can be analytically detected by conventional chromatographic techniques. ESR is currently the most effective research method for detecting free radicals. It is simple, effective, intuitive, and clear. 5,5-Dimethyl-1-pyrroline-*N*-oxide (DMPO) has become the most commonly used trapping agent in ESR detection of •OH due to its high selectivity for •OH.[6,7] DMPO rapidly reacts with hydroxyl radicals, forming a relatively stable spin addition product, DMPO-OH. The ESR technique can detect the signal of DMPO-OH, generating highly identifiable characteristic spectral lines. The intensities of these signal spectral lines can indirectly indicate the relative production of hydroxyl

Received: September 19, 2024
Revised: November 10, 2024
Accepted: November 14, 2024
Published: December 3, 2024

radicals. However, spin scavengers may lead to false positive detection of •OH,[8−10] which is attributed to reverse spin scavenging,[11,12] or the Forrester−Hepburn mechanism.[9,10] False positive detection of hydroxyl radicals makes it difficult to accurately characterize their concentration. Existing qualitative and quantitative detection methods for hydroxyl radicals have some deficiencies, and their reliability needs to be further improved. Therefore, the ESR method can only qualitatively and semiquantitatively determine hydroxyl radicals.

Martínez-Huitle investigated the electrochemical behavior of oxalic acid on various electrodes. It was observed that the BDD electrode exhibits a very low adsorption capacity and high stability to oxidation on the surface. This characteristic allows reactants and intermediates to undergo reactions in a nonadsorbent state, suggesting that hydroxyl radicals may react with oxalic acid on this electrode.[13] Subsequently, the electro-oxidation reaction of oxalic acid was investigated on the BDD electrode. The Tafel slope was found to be within the range of 200−240 mV decade^{-1}, and the reaction order was slightly less than 0.55. There are also many studies on electro-oxidation on BDD electrodes. For example, some scholars used cyclic voltammetry and bulk electrolysis to study the anodic oxidation of 2-naphthol on a synthetic BDD electrode in acidic media and established a model to explore the electrooxidation mechanism, in which •OH plays an important role.[14] The electrochemical oxidation of iohexol on BDD electrodes has also been studied, and the current efficiency and COD elimination rate are consistent with the theoretical model proposed by Comninellis et al. that assumes mass transfer control.[14−16]

This study marks the initial utilization of the BDD electrode for electrochemical investigations on oxalic acid in a nitric acid medium. ESR spectroscopy was employed to detect the electrogenerated hydroxyl radical on the BDD electrode, and an AC impedance test was carried out; then the process conditions were explored. This study aimed to ascertain the mechanism of the electrooxidation of oxalic acid in a nitric acid medium using a BDD electrode. Through this, the study sought to preliminarily explore the potential application of the BDD electrode in the nuclear fuel reprocessing process.

2. EXPERIMENTAL SECTION

2.1. Instruments and Reagents. The electrochemical experiments were conducted using a CHI-760E Electrochemical Workstation and a CHI-1140C Electrochemical Workstation, both from Shanghai Chenhua Instrument Co., Ltd. The analytical balance employed was a GB204 Analytical Balance by METTLER TOLEDO, with an accuracy of 10^{-4} g. An MS-5000 Spectrometer from Magnettech, Germany, was utilized for electron paramagnetic resonance spectroscopy. The concentration of trace oxalic acid was analyzed using the ICS-5000 ion chromatograph produced by ThermoFisherScientific, USA. Additionally, ultrapure water was obtained using the Direct-Q 3UV Ultra-Pure Water Machine by Millipore Corporation. The chemicals used in the experiments were sourced from reputable suppliers: oxalic acid dihydrate and potassium nitrate were obtained in analytically pure form from Sinopharm Group. Nitric acid with a mass fraction of 65%−68%, classified as analytically pure, was acquired from Sinopharm Group. Concentrated sulfuric acid with a mass fraction of 95%−98%, also analytically pure, was sourced from the Sinophosphate Group. 5,5-Dimethyl-1-pyrroline-*N*-oxide (DMPO, with a purity of 97%) was procured from Shanghai McLean Reagent and was analytically pure.

2.2. Experimental Methods. The procedure involves quantitatively weighing solid oxalic acid and dissolving it in various nitric acid concentrations to create a mixed solution. Ultrapure water was used in the preparation of the solution. Before use, the BDD electrode was rinsed several times with deionized water. Three electrodes were employed in the experiment: the working electrode, BDD electrode (10 mm × 10 mm), the counter electrode, platinum electrode (10 mm × 10 mm), and the reference electrode is saturated calomel electrode (SCE). Unless stated otherwise, the saturated calomel electrode was utilized as the reference electrode and all electrochemical studies were carried out at room temperature.

The constant-current electrolysis method was implemented by using the CHI-1140C electrochemical workstation to perform the electrolysis of oxalic acid at various current densities. The concentration of $H_2C_2O_4$ was determined through $KMnO_4$ titration with timed sampling. The electrolytic cell, designed and fabricated in-house, was constructed entirely from an acrylic material. The cell features a groove to accommodate the electrodes.

To minimize DMPO consumption and enhance the •OH concentration in the sample, an electrolytic cell with a plate spacing of 1 cm was employed. A Nafion 117 diaphragm was placed in the middle of the electrolytic cell to prevent interference from materials generated at the cathode. The ESR experimental setup included a working electrode composed of BDD (2 cm × 4 cm), an auxiliary electrode made of graphite (2 cm × 4 cm). And the reference electrode was also a saturated calomel electrode. The BDD and graphite sheet electrodes were partially immersed in the solution, with an immersion area of 2 cm × 3 cm.

Before each experiment, a blank sample was prepared by combining DMPO and the electrolyte in an unpowered state. The mixture, consisting of 6.3 mL of electrolyte, was subjected to ESR testing. This involves using DMPO as a spin trap to capture •OH in the system, adjusting to various electrochemical oxidation reaction conditions.

The measurement parameters of •OH in the X-band were configured as follows: the center field is set at 336.7 mT, the scanning width is 10 mT, the scanning time is 30 s, the microwave frequency is 9.49 GHz, the microwave power is 20 mW, the modulation amplitude is 0.1 mT, and the modulation frequency is 100 kHz.

3. RESULTS AND DISCUSSION

3.1. Electrochemical Response of Oxalic Acid on a BDD Electrode. This experiment utilized a titanium-based boron-doped diamond electrode imported from Beijing BOLTARA Technologies Co., Ltd., Germany. Scanning electron microscopy (SEM) was employed to observe this electrode's morphology to comprehend its microstructure. Figure 1 illustrates the side and plane views of the BDD electrode.

Figure 1a,b show approximately 120-μm-thick boron-doped diamond coatings on both sides of the Ti substrate, displaying high density and uniformity. The magnified image at the junction of Figure 1c further illustrates the tight and compact nature of the coating. In Figure 1 d−i, a flat view is depicted, showcasing a highly dense structure. The presence of "small

https://doi.org/10.1021/acsomega.4c08628
ACS Omega 2024, 9, 49839−49848

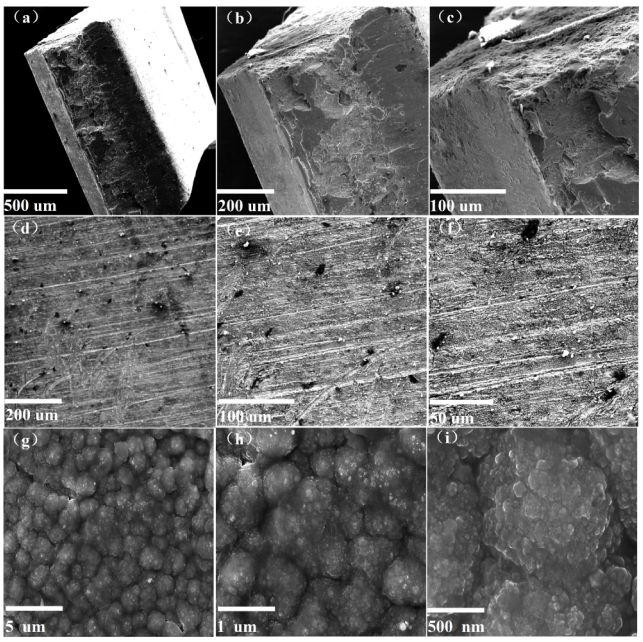

Figure 1. (a) SEM image of the entire surface of the BDD electrode (scale bar: 500 μm), (b) SEM image of the side view of the BDD electrode (scale bar: 200 μm), (c) SEM image of the local amplification of the BDD electrode side (scale bar: 100 μm), (d) SEM image of the plane of the BDD electrode (scale bar: 200 μm), (e) SEM image of the plane of the BDD electrode (scale bar: 100 μm), (f) SEM image of the plane of the BDD electrode (scale bar: 50 μm), (g) SEM image of the plane of the BDD electrode (scale bar: 5 μm), (h) SEM image of the plane of the BDD electrode (scale bar: 1 μm), and (i) SEM image of the plane of the BDD electrode (scale bar: 500 nm).

black pits" on the surface is attributed to spark splashing during laser cutting, leading to surface damage on the BDD electrode.

A cyclic voltammetry curve was generated by varying the oxalic acid concentration, as depicted in Figure 2a, to identify the position of the oxalic acid oxidation peak. It is evident that with the rise in oxalic acid concentration, the increase in the oxidation peak is minimal. A faint oxidation peak is observed at 1.0 V vs SCE, occurring before the onset of the oxygen evolution reaction.

In order to investigate the impact of adding nitric acid on the oxidation of oxalic acid, the cyclic voltammetry curve depicting oxalic acid with increasing nitric acid concentration is presented in Figure 2b. As the nitric acid concentration increases, the oxidation current of oxalic acid shows no significant decrease near 1.0 V vs SCE. However, the oxidation decomposition current of water notably decreases near 1.8 V vs SCE. On the BDD electrode, water oxidation and decomposition produce a substantial amount of $^{\bullet}$OH.[17] The oxidation of organic matter on the BDD electrode relies on the indirect oxidation facilitated by $^{\bullet}$OH.[18,19] Considering the potent oxidation capacity of $^{\bullet}$OH, it can oxidize and decompose oxalic acid effectively. Following the reaction $H_2O \rightarrow {}^{\bullet}OH + H^+ + e^-$, an increase in the nitric acid concentration shifts the balance to the left, decreasing the production of $^{\bullet}$OH. The reduction in current indicates a decrease in the rate of $^{\bullet}$OH generation. Therefore, the addition of nitric acid is not conducive to the oxidation of oxalic acid at the BDD electrode.

3.2. Study on the Detection and Formation Mechanism of Electrogenic Hydroxyl Radicals on BDD Electrode. *3.2.1. Effect of Voltage on the Generation of Hydroxyl Radicals.* Until now, limited studies have identified electrically generated $^{\bullet}$OH by DMPO in electrochemical systems.[20] Research indicates two primary reasons for the challenges encountered in obtaining successful results: (I) Theoretically, to generate $^{\bullet}$OH, the anode potential should surpass the oxygen evolution potential. However, the direct electron transfer reaction (DET) of DMPO may also inevitably occur on the anode, rendering it unable to capture $^{\bullet}$OH qualitatively. The oxidation potential of DMPO in aqueous solution is challenging to determine, as only the oxidation potential of DMPO in nonaqueous solution is established at 1.87 V vs SHE;[8] (II) the spin adduction of DMPO-OH is chemically unstable, and subsequent transformations, including dimerization, disproportionation, DET oxidation, and further oxidation, may occur in the strong oxidation environment facilitated by anode polarization. In order to obtain effective spin trapping of $^{\bullet}$OH and reliable ESR signals of DMPO-OH

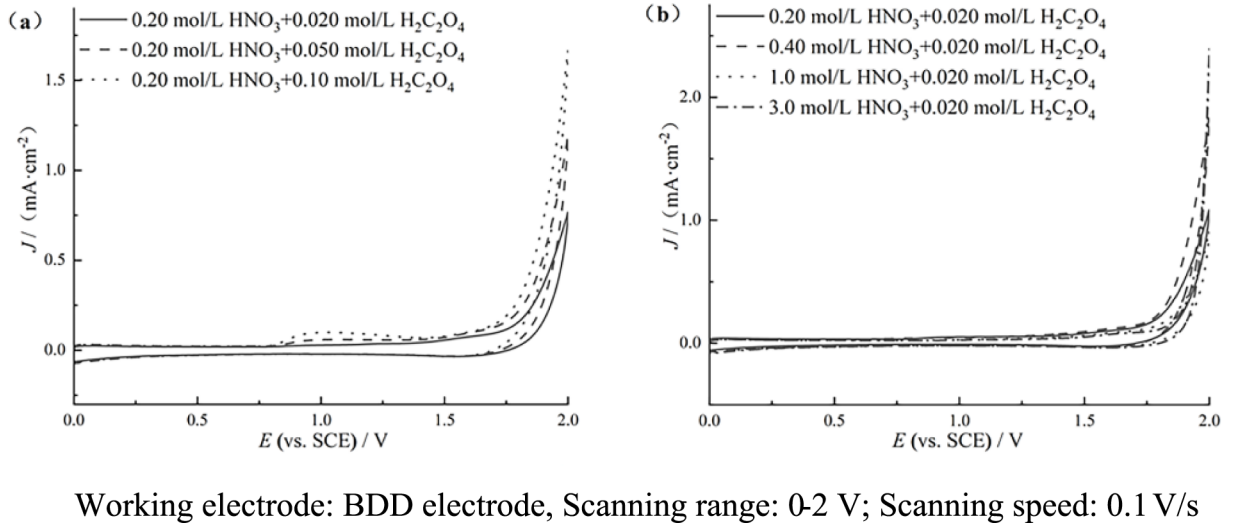

Figure 2. (a) Cyclic voltammograms of 0.20 mol/L HNO_3 and different concentrations of $H_2C_2O_4$. (b) Cyclic voltammograms of 0.020 mol/L $H_2C_2O_4$ and different concentrations of HNO_3.

https://doi.org/10.1021/acsomega.4c08628
ACS Omega 2024, 9, 49839−49848

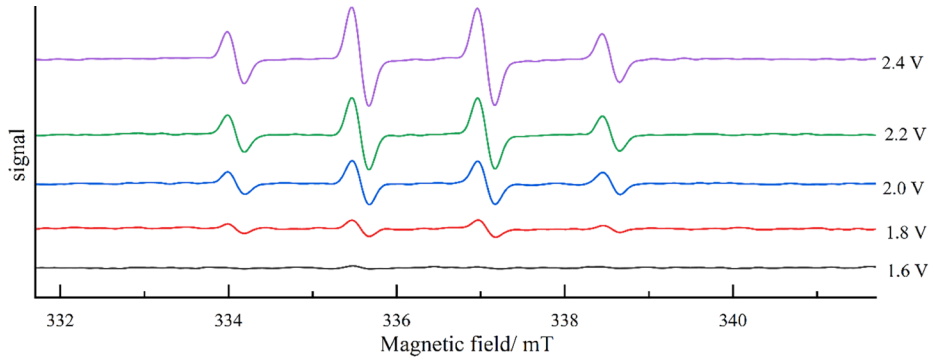

Figure 3. ESR signal spectra at different voltages on the BDD electrode.

adducts, side reactions between DMPO and DMPO-OH adducts should be minimized, which can be achieved by adding excessive DMPO during the trapping of electro-generated •OH. Therefore, all DMPO stock solutions are put into the electrolytic cell, and the amount added is fixed at 50 μL each time.

In the electrolysis process, •OH can be captured using DMPO only when the applied potential is greater than the potential generated by the hydroxyl radical; the standard potential for •OH radical formation is 2.38 V vs SHE. Figure 2 illustrates that the potential of hydroxyl radicals generated during water electrolysis in the presence of 0.20 mol/L HNO_3 + 0.020 mol/L $H_2C_2O_4$ electrolyte on the BDD electrode is 1.8 V vs SCE. The working electrode was the BDD electrode, with a graphite plate as the auxiliary electrode. The electrolyte consisted of 0.20 mol/L HNO_3 + 0.020 mol/L $H_2C_2O_4$ and 50 μL of DMPO. The DMPO stock solution was introduced before initiating electrolysis, and experiments were conducted at varying voltages. The voltage settings for the experiment were 1.6 V vs SCE, 1.8 V vs SCE, 2.0 V vs SCE, 2.2 V vs SCE, and 2.4 V vs SCE, with ESR testing conducted at the fourth minute sampling interval. The outcomes of the experiment are depicted in Figure 3.

In Figure 3, the detected free radical spectrum exhibits a peak height ratio of 1:2:2:1, with a g factor of 2.007 and hyperfine structure parameters of approximately α_N = 1.51 mT and α_H = 1.51 mT. These parameters closely align with the characteristic peak of •OH, as reported in the literature.[17] Consequently, it is established as the characteristic signal peak of the DMPO-OH adduct.

To facilitate a clearer comparison of the DMPO-OH adduct signal heights at different voltages on the BDD electrode in Figure 3, a curve was generated as depicted in Figure 4. This curve represents the signal value at each voltage when the magnetic field is set at 335.5 mT.

As depicted in Figure 4, when the potential is 1.6 V vs SCE, there is virtually no characteristic signal of DMPO-OH. However, from 1.8 V vs SCE to 2.4 V vs SCE, the signal intensity of DMPO-OH steadily increases in the ESR test. This indicates that the concentration of the DMPO-OH adduct also increases, signifying an elevated production of •OH with increased potential. This observation validates that for •OH to be generated on the surface of the BDD electrode, the anode potential must reach at least +1.8 V vs SCE.

3.2.2. Effect of Nitric Acid Concentrations on the Generation of Hydroxyl Radicals. The concentration of nitric acid plays a crucial role in the electrolytic oxidation of oxalic acid. Consequently, various concentrations of nitric acid were

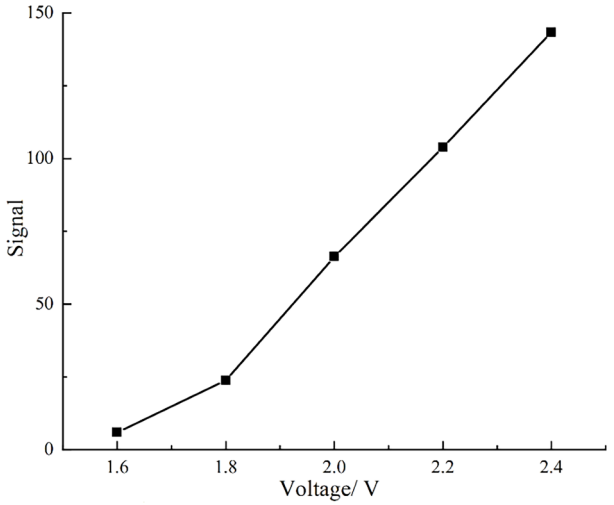

Figure 4. ESR signal values of the BDD electrode at different voltages with a constant magnetic field of 335.5 mT.

systematically examined here to assess their influence on the production of hydroxyl radicals. The experimental setup involved using the BDD electrode as the working electrode and the graphite sheet as the auxiliary electrode and introducing 0.020 mol/L $H_2C_2O_4$, 0.20 mol/L HNO_3 + 0.020 mol/L $H_2C_2O_4$, 0.40 mol/L HNO_3 + 0.020 mol/L $H_2C_2O_4$, 1.0 mol/L HNO_3 + 0.020 mol/L $H_2C_2O_4$, 3.0 mol/L HNO_3 + 0.020 mol/L $H_2C_2O_4$, respectively, and 50 μL of DMPO as the electrolyte before initiating the electrolysis. The electrolysis experiments were conducted at a constant current density of 60 mA cm^{-2}. The ESR testing was performed at fourth minute of electrolysis. The outcomes of the experiments are presented in Figure 5.

A curve was generated to facilitate a clear comparison of the DMPO-OH signal height on the BDD electrode under different nitric acid concentrations, as depicted in Figure 6. This curve represents the signal value of each nitric acid concentration when the magnetic field is set at 335.5 mT.

As observed in Figures 5 and 6, the signal intensity of DMPO-OH in 0.020 mol/L $H_2C_2O_4$ without nitric acid is lower than that in 0.20 mol/L HNO_3 + 0.020 mol/L $H_2C_2O_4$. This suggests that a low nitric acid concentration is favorable for the formation of •OH. Studies have shown that compared with alkaline environments, OH oxidation is stronger under acidic conditions.[21]

With the gradual increase in nitric acid concentration, the signal intensity of DMPO-OH gradually decreases, signifying a

https://doi.org/10.1021/acsomega.4c08628
ACS Omega 2024, 9, 49839−49848

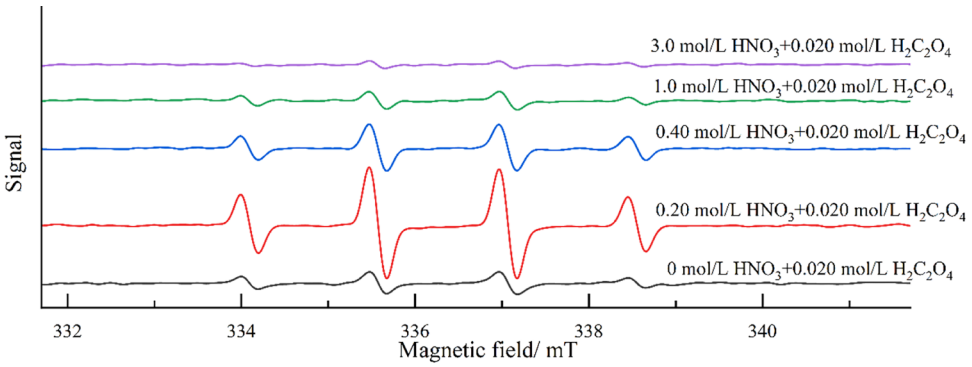

Figure 5. ESR signal spectra at different nitric acid concentrations on the BDD electrode.

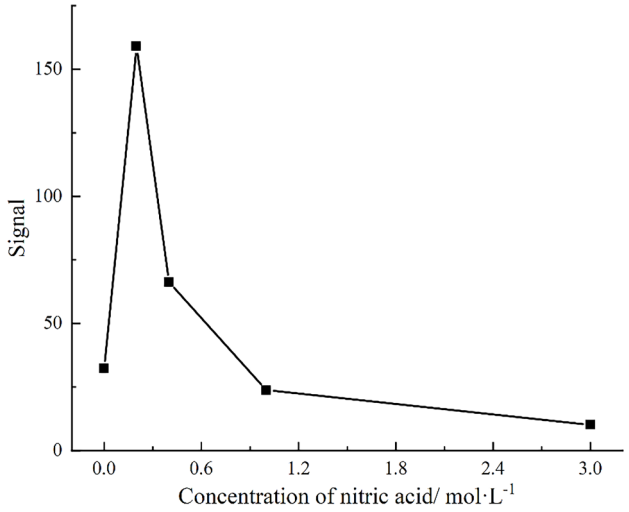

Figure 6. ESR signal values of the BDD electrode at different nitric acid concentrations, measured at 335.5 mT.

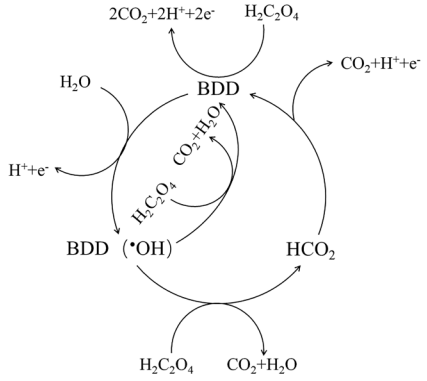

Figure 7. Schematic diagram illustrating the oxidation mechanism of oxalic acid at the BDD electrode.

gradual reduction in the concentration of •OH. This indicates that the progressive increase in nitric acid concentration inhibits the production of •OH. An excessive amount of H^+ shifts the equilibrium of $H_2O \rightarrow {}^{\bullet}OH + H^+ + e^-$ to the left, decreasing the amount of •OH produced. It is worth noting that the oxidation of DMPO is also affected by pH,[10,22,23] the pH value also affects the stability of DMPO-OH, so the reasons for such fluctuations in the signal may be caused by many aspects and require further investigation. However, as the acidity gradually increased, the DMPO-OH signal intensity first increased and then decreased, which was consistent with the conclusion presented in Figure 2b, that is, too high of an acidity was not conducive to the electrooxidation of oxalic acid.

Based on the findings in Figure 2a,b and the results of the ESR test, the inferred oxidation mechanism of oxalic acid on the BDD electrode in the nitric acid system is illustrated in Figure 7.

The electrooxidation of oxalic acid on the BDD electrode leads to the production of CO_2, representing the direct electron transfer step. The indirect oxidation involving •OH is manifested in the generation of •OH through water electrolysis at the BDD electrode, followed by its adsorption on the electrode. An increase in the nitric acid concentration reduces the overall quantity of •OH generated in this reaction. Subsequently, the adsorbed free radical reacts with oxalic acid to produce HCO_2, CO_2, and H_2O. Additionally, HCO_2 reacts with the BDD electrode to generate CO_2. The reaction of adsorbed •OH with oxalic acid also directly yields CO_2 and H_2O.

3.3. AC Impedance Characteristics of Oxalic Acid on BDD Electrode in Nitric Acid Medium. The AC impedance test in this experiment was conducted using an electrochemical workstation CHI-760E. A small-amplitude AC positive voltage of 5 mV was the perturbation signal. Moreover, the frequency ranged from 0.01 to 100,000 Hz. The AC impedance of a 0.20 mol/L HNO_3 + 0.020 mol/L $H_2C_2O_4$ solution was measured using the BDD electrodes as working electrodes at the open-circuit voltage.

Figure 8 represents the Nyquist diagram of oxalic acid in a nitric acid medium on the BDD electrode. Typically, AC impedance measurement results are fitted to an equivalent circuit. This circuit represents the physical processes transpiring in the entire electrochemical reaction system, encapsulating the comprehensive electrical characteristics of the electrochemical system. The elements within it can elucidate the properties of the solution. However, a single element in the fitting circuit does not always accurately portray the system's genuine physical and chemical characteristics. The circuit diagram is illustrated in Figure 9.

In Figure 9, R1 symbolizes the solution resistance in the system, Rct represents the electrochemical reaction charge transfer resistance, Rdm denotes the BDD electrode resistance, Cdm refers to the double-layer capacitance of the BDD electrode, and Cdl signifies the double-layer capacitance of the solution. The fitting results are presented in Table 1, demonstrating close alignment with the actual physical and chemical parameters. The electric double-layer capacitance of

https://doi.org/10.1021/acsomega.4c08628
ACS Omega 2024, 9, 49839−49848

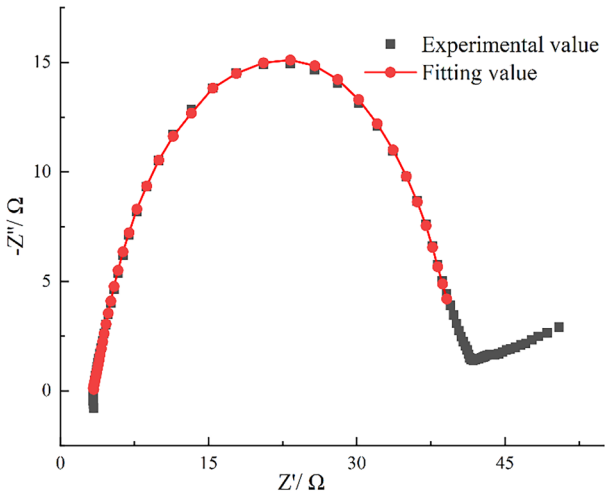

Figure 8. Nyquist diagram and fitting diagram for 0.20 mol/L HNO_3 + 0.020 mol/L $H_2C_2O_4$ on the BDD electrode.

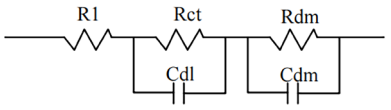

Figure 9. Equivalent circuit diagram corresponding to the Nyquist diagram using 0.20 mol/L HNO_3 + 0.020 mol/L $H_2C_2O_4$ on the BDD electrode.

Table 1. Simulation Results of the Equivalent Circuit on the BDD Electrode

R1/Ω	Rct/Ω	Rdm/Ω	Cdl/F	Cdm/F
3.6	2.6	31.6	8.0×10^{-5}	8.2×10^{-5}

the boron-doped diamond electrode is comparable to the values obtained by Yoshimura et al.[24]

In the Nyquist diagram, a smaller semicircle diameter and lower Rct correspond to smaller charge transfer resistance for oxalic acid oxidation. Consequently, oxalic acid in a nitric acid medium exhibits a high reaction rate on the BDD electrode. This observation aligns with the mechanism of the BDD electrode oxidizing oxalic acid. The oxidation of oxalic acid on the BDD electrode occurs via two pathways. One is the direct oxidation of oxalic acid on the electrode, playing a secondary role. The other is the oxidation of oxalic acid by hydroxyl radicals generated by the BDD electrode, which plays a primary role.

3.4. Studies on Electrolysis of Oxalic Acid in Nitric Acid Medium. *3.4.1. Influence of Current Density on the Electrolysis of Oxalic Acid.* The BDD electrode was employed to investigate various factors influencing the electrolysis of oxalic acid in a nitric acid medium. These factors include the current density, initial nitric acid concentration, initial oxalic acid concentration, and different plate spacings. The study aimed to optimize the process conditions for the electrolysis of oxalic acid and provide a preliminary discussion on the electrolytic kinetic characteristics of $H_2C_2O_4$.

Current density is a crucial factor influencing the electrolytic rate and the operational costs. To examine the impact of oxalic acid electrolysis using the BDD electrode under various current densities, the following settings were applied: 20 mA cm^{-2}, 40 mA cm^{-2}, 60 mA cm^{-2}, and 90 mA cm^{-2}. The electrolytes for all cases were 3.0 mol/L HNO_3 + 0.30 mol/L $H_2C_2O_4$, with other conditions kept constant. The oxalic acid removal rate during electrolysis under different current densities is illustrated in Figure 10. As the current density increases, the

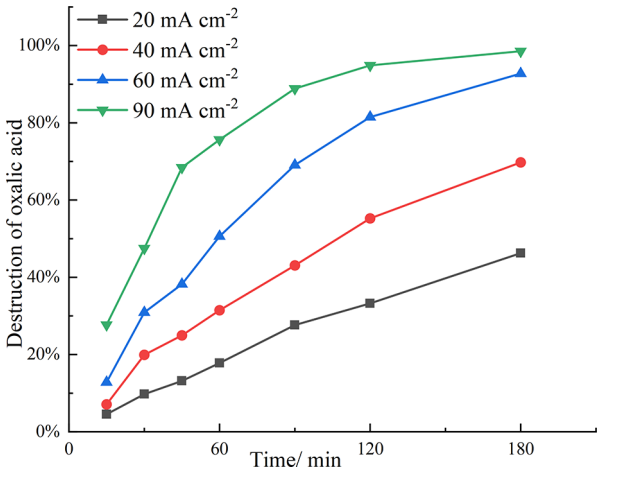

Figure 10. Effect of Current Densities on the electrolysis of oxalic acid.

destruction rate of oxalic acid gradually rises within the same time frame. Moreover, the higher the current density, the more potent the ability to degrade oxalic acid. At a current density of 20 mA cm^{-2}, the removal of oxalic acid is notably slow. However, at current densities of 60 mA cm^{-2} and 90 mA cm^{-2}, the removal rates reached 93% and 98%, respectively, after 180 min. Despite the current density of 90 mA cm^{-2} being 50% higher than that of 60 mA cm^{-2}, the final removal rate of oxalic acid is only 5% higher. This suggests a higher energy loss at a higher current density. Consequently, a current density of 60 mA cm^{-2} is deemed more suitable as the process condition for subsequent electrolysis.

Current density serves as an indicator of the electrochemical reaction rate. Therefore, the reaction kinetics of oxalic acid degradation under different current densities were examined, and the results are depicted in Figure 11. The degradation of oxalic acid by the BDD electrode at different current densities follows a quasi-first-order reaction. The apparent reaction rate constant gradually increases from 0.0035 min^{-1} at 20 mA cm^{-2} to 0.0240 min^{-1} at 90 mA cm^{-2}. The increase in current density leads to higher energy input into the oxalic acid system in the nitric acid medium. Consequently, there is an increase in the total amount of $^{\bullet}OH$ produced through electrolysis on the surface of the BDD electrode. This increase enhances the probability of contact between oxalic acid and $^{\bullet}OH$, accelerating the reaction rate between $^{\bullet}OH$ and oxalic acid and resulting in a more effective degradation of oxalic acid.

The current efficiency under different current densities is calculated, and the results are presented in Table 2.

As indicated in Table 2, the current efficiency experiences a gradual decline with the increase of current density.

The first reason for this phenomenon is that under higher current conditions, electrolytic products may not have sufficient time to detach from the electrode surface, and reactants may not diffuse to the electrode promptly, resulting in a decrease in current efficiency. Second, typically at low current densities, there is no noticeable formation of hydroxyl radicals in the electrolytic cell, and the $^{\bullet}OH$ produced primarily reacts with the target for degradation or some

https://doi.org/10.1021/acsomega.4c08628
ACS Omega 2024, 9, 49839−49848

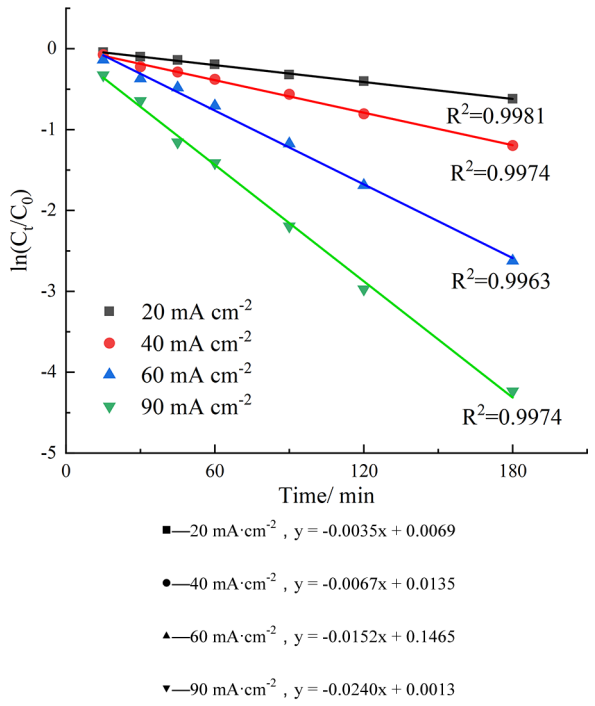

Figure 11. Relation between electrolytic oxalate ln (C_t/C_0) and reaction time at different current densities.

Table 2. Current Efficiency of Electrolytic Oxalic Acid at Different Current Densities

Current density/mA cm^{-2}	Current efficiency (%)
20	48.8
40	35.2
60	30.5
90	21.5

intermediate products. However, the surplus $^{\bullet}OH$ does not react with the degradation substance as the current density increases. However, it consumes itself, leading to an oxygen evolution side reaction,[25] as illustrated in eq 1.

$$2^{\bullet}OH \rightarrow O_2 + 2H^+ + 2e^- \quad (1)$$

With the escalation of the oxygen evolution side reaction, the proportion of current utilized for the degradation of the target pollutant in the increased current reduces. This decrease results in a reduction in the current efficiency. At a current density of 60 mA cm^{-2}, the current efficiency is only slightly less than 5% lower than that at 40 mA cm^{-2}, but it is 9% higher than the 21.5% observed at 90 mA cm^{-2}. Therefore, a current density of 60 mA cm^{-2} is more suitable for subsequent electrolysis. Considering the degradation rate, reaction rate, and current efficiency of oxalic acid under different current densities, 60 mA cm^{-2} was chosen as the suitable current density for the subsequent electrolysis process.

3.4.2. Effect of Nitric Acid Concentration on the Electrolysis of Oxalic Acid. All other conditions remained unchanged at a constant current density of 60 mA cm^{-2}. The impact of different concentrations of nitric acid on the electrolysis of oxalic acid was investigated by using the BDD electrode, and the results are depicted in Figure 12. From the graph, it is evident that there is minimal difference in the curve of oxalic acid destruction rate over time from 0.50 mol/L HNO_3 to 3.0 mol/L HNO_3. Only the curve of the oxalic acid

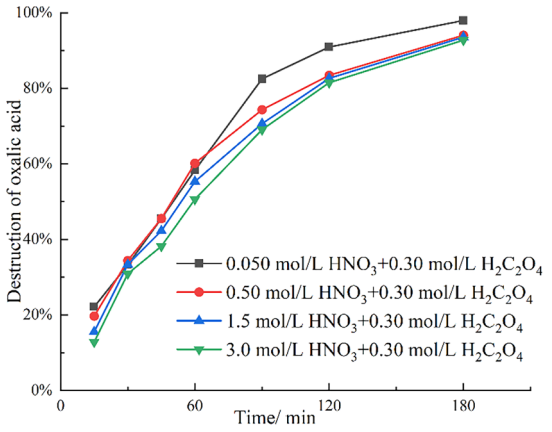

Figure 12. Effect of nitric acid concentrations on the electrolysis of oxalic acid.

destruction rate over time at 0.050 mol/L HNO_3 is higher than the other three curves after 90 min. Furthermore, the oxalic acid destruction rate exceeds 92% under these four nitric acid concentrations at 180th minute. The curve corresponding to 0.050 mol/L of HNO_3 achieves a 98% oxalic acid destruction rate.

Further investigation was conducted into the reaction kinetics of oxalic acid and its degradation under different nitric acid concentrations, and the resulting curve is depicted in Figure 13. Figure 13 reveals that as the concentration of nitric acid in the system increases sequentially from 0.050 to 3.0 mol/L, the corresponding apparent reaction rate constants are 0.0228 min^{-1}, 0.0158 min^{-1}, 0.0156 min^{-1}, and 0.0152 min^{-1}. Consequently, the reaction rate of BDD electrode degradation of oxalic acid in the nitric acid system decreases with the increase of nitric acid concentration. This suggests that an

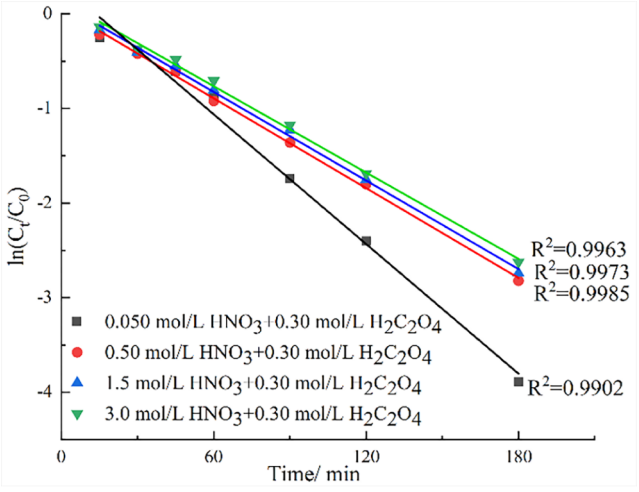

Figure 13. Correlation between ln(C_t/C_0) of oxalic acid electrolyzed with different nitric acid concentrations and reaction time.

https://doi.org/10.1021/acsomega.4c08628
ACS Omega 2024, 9, 49839−49848

increase in nitric acid concentration hinders the electrolysis of oxalic acid. This observation aligns with the findings from a previous study utilizing cyclic voltammetry on the BDD electrode to investigate the impact of nitric acid on oxalic acid electrolysis. An excess of H^+ diminishes the level of production of $^{\bullet}OH$, leading to a decrease in the reaction rate with oxalic acid. Consequently, increasing nitric acid concentration progressively reduces the BDD electrolytic oxalic acid's apparent reaction rate constant.

3.4.3. Effect of Initial Concentration of Oxalic Acid on the Electrolysis of Oxalic Acid. At ambient temperature, maintaining a constant current density of 60 mA cm^{-2}, electrolysis was conducted in 3.0 mol/L HNO_3 solutions with different initial oxalic acid concentrations using BDD electrodes. The results are depicted in Figure 14, revealing variations in the removal rate of oxalic acid with different initial concentrations within the first 90 min, with the destruction rate slowing after 45th minute.

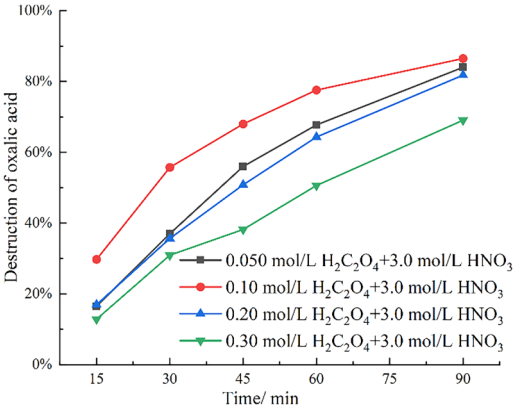

Figure 14. Effect of initial oxalic acid concentrations on the electrolysis of oxalic acid.

Further investigation was conducted into the reaction kinetics of oxalic acid degradation at different initial concentrations. The resulting curve is depicted in Figure 15. Analysis of Figure 15 reveals that as the initial concentration of oxalic acid in the system increases from 0.050 to 0.30 mol/L, the corresponding apparent reaction rate constants are 0.0222 min^{-1}, 0.0235 min^{-1}, 0.0213 min^{-1}, and 0.0152 min^{-1}. Hence, the reaction rate of oxalic acid degradation in the nitric acid system by the BDD electrode initially increased and then decreased with the increase in initial concentration. This phenomenon could be attributed to the extremely short existence time of $^{\bullet}OH$ in the aqueous phase, lasting approximately 10^{-9} s. Under specific initial conditions of the electrolytic system, the total amount of $^{\bullet}OH$ produced on the surface of the BDD electrode remains constant for a certain time. When the oxalic acid concentration in the system is low, the probability of $^{\bullet}OH$ molecules coming into contact with oxalic acid molecules is relatively low, within their very short lifetimes. As a result, the reaction rate is limited. However, as the oxalic acid concentration increases slightly, a sufficient amount of $^{\bullet}OH$ becomes available, leading to an increased interaction with oxalic acid and an elevated reaction rate. However, when the concentration of oxalic acid is too high, the total amount of $^{\bullet}OH$ produced on the surface of the BDD electrode becomes significantly lower than that of the oxalic acid. Consequently, there is insufficient $^{\bullet}OH$ to effectively

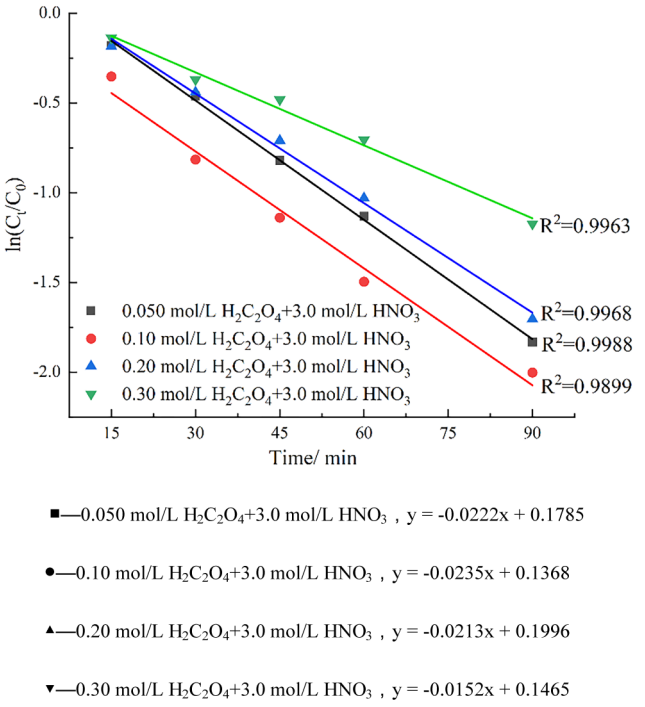

Figure 15. Correlation between electrolytic $\ln(C_t/C_0)$ of oxalic acid and reaction time at different initial oxalic acid concentrations.

interact with oxalic acid for degradation. In essence, the system's degradation capability is weakened at high oxalic acid concentrations, leading to a decrease in the reaction rate.

3.4.4. Effect of Plate Spacing on the Electrolysis of Oxalic Acid. Certainly, the electrode spacing is a crucial parameter in the electrolysis process. Therefore, a BDD electrode was used, and the fixed current density was 60 mA cm^{-2} at room temperature. Figure 16 displays the curves depicting the

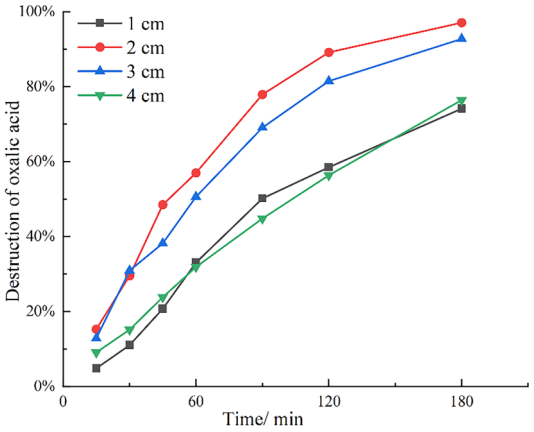

Figure 16. Effect of the spacings on the electrolysis of oxalic acid.

changes in the oxalic acid electrolytic destruction rate over time at various plate spacings. Notably, the oxalic acid failure rate is significantly higher for plate spacings of 2 and 3 cm compared to 1 and 4 cm. Additionally, the electrolytic failure rate at a 2 cm plate spacing is superior to that at 3 cm.

The investigation of the reaction kinetics of oxalic acid degradation at different initial concentrations is further explored, and the resulting curve is depicted in Figure 17. It illustrates that the oxidation degradation of oxalic acid by the

https://doi.org/10.1021/acsomega.4c08628
ACS Omega 2024, 9, 49839−49848

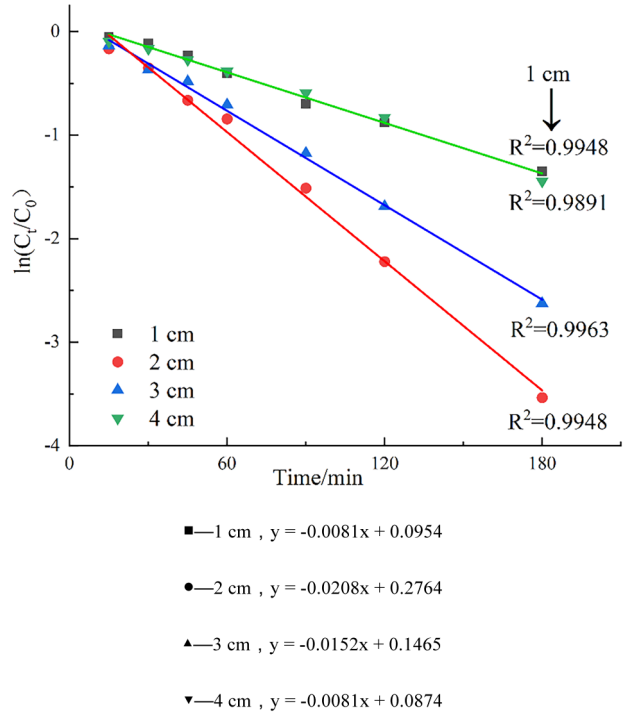

Figure 17. Relationship between the electrolytic $\ln(C_t/C_0)$ of oxalic acid and reaction time for various plate spacing.

BDD electrode adheres to a quasi-first-order reaction under different plate spacings, with varying apparent reaction rate constants. The apparent reaction rate constant peaks at a plate spacing of 2 cm, measuring 0.0208 min^{-1}. In contrast, the apparent reaction rate constants for plate spacings of 1 and 4 cm are consistent, registering at 0.0081 min^{-1}. This suggests that a plate spacing of 2 cm is the most suitable configuration for the electrolysis of oxalic acid. The performance of proton transfer during electrolysis is affected by the spacing between the electrode plates. In general, the smaller the plate spacing of the electrodes, the better the effect achieved by electrolyzing the target substance. However, if the distance between the electrode plates is too close, the treatment effect will be reduced, and in severe cases, the risk of a short circuit between the electrodes may also be caused.

The most suitable current density and plate spacing for electrolysis were explored in the previous article. In order to explore the extent to which the BDD electrode can destroy oxalic acid, the BDD electrode is used as the working electrode, and the graphite sheet electrode is used as the auxiliary electrode. The submerged area of the two electrodes is consistent with the previous work, and the saturated calomel electrode is used as the reference electrode. The electrolysis current density is set to 60 mA cm^{-2}, the electrode plate spacing is 2 cm, and constant current electrolysis is carried out on 0.040 mol/L KCl + 0.010 mol/L $H_2C_2O_4$. The oxalic acid concentration in the sample is detected using an ion chromatograph. The results are listed in Table 3.

It can be seen from Table 3 that the BDD electrode can destroy the oxalic acid concentration to below 0.001 mol/L, which meets the process requirement that the residual oxalic acid concentration in the plutonium oxalate mother liquor is less than 0.001 mol/L.

Table 3. Oxalic Acid Concentration at Different Electrolysis Times

Electrolysis time/min	Oxalic acid concentration / mol L^{-1}
30	6.92×10^{-3}
60	1.53×10^{-3}
150	3.12×10^{-4}

4. CONCLUSIONS

In order to investigate the feasibility of using electrooxidation to destroy oxalic acid in plutonium oxalate mother liquor, the electrochemical behavior of oxalic acid in a nitric acid medium on the BDD electrode was studied, and combined with ESR method detection of DMPO-OH, the mechanism of electrooxidation of oxalic acid in a nitric acid medium was speculated. It was found that hydroxyl radicals play a major role in oxidizing oxalic acid, and direct oxidation of oxalic acid by the electrode plays a minor role. Moreover, too high of a concentration of nitric acid will reduce the electrooxidation rate of oxalic acid, which is also supported in subsequent electrolysis process optimization research. An AC impedance test was carried out on oxalic acid in a nitric acid medium using a BDD electrode. The electric double-layer capacitance of the BDD electrode was determined to be 8.2×10^{-5} F, and the AC impedance test proved that the BDD electrode electrolyzes oxalic acid quickly. Ion chromatography was used to detect the concentration of trace oxalic acid, and it was found that the BDD electrode could finally destroy the oxalic acid concentration to below 0.001 mol/L, meeting the process requirement. This substantiates the potential application of BDD electrodes in the electrolysis of oxalic acid in the plutonium oxalate mother liquor, offering an efficient means of degrading oxalic acid without the introduction of additional waste products.

AUTHOR INFORMATION

Corresponding Author

Hu Zhang − *China Institute of Atomic Energy, Beijing 102413, China;* orcid.org/0000-0003-2979-7300; Email: ciaezhhu@163.com

Authors

Lu Qiao − *China Institute of Atomic Energy, Beijing 102413, China;* orcid.org/0000-0002-5012-1658

Jing Zhao − *China Institute of Atomic Energy, Beijing 102413, China*

Zhijun Cen − *China Institute of Atomic Energy, Beijing 102413, China*

Ting Yu − *China Institute of Atomic Energy, Beijing 102413, China*

Complete contact information is available at: https://pubs.acs.org/10.1021/acsomega.4c08628

Notes

The authors declare no competing financial interest.

ACKNOWLEDGMENTS

The paper is sponsored by the National Natural Science Foundation of China (U1867205) and the Special Project on Spent Fuel Reprocessing of the State Administration of Science, Technology and Industry for National Defence (BG222512000403).

https://doi.org/10.1021/acsomega.4c08628
ACS Omega 2024, 9, 49839−49848

REFERENCES

(1) Pines, D. S.; Reckhow, D. A. Effect of dissolved cobalt(II) on the ozonation of oxalic acid. *Environ. Sci. Technol.* **2002**, *36* (19), 4046.

(2) Kim, E. H.; Chung, D. Y.; Kwon S, W.; Yoo, J. H. Photochemical decomposition of oxalate precipitates in nitric acid medium. *Korean J. Chem. Eng.* **1999**, *16* (3), 351−356.

(3) Mailen, J. C.; Tallent, O. K.; Arwood, P. C. *Destruction of oxalate by reaction with hydrogen peroxide*. Ornl/TM-7474, 1981.

(4) Ganesh, S.; Desigan, N.; Chinnusamy, A.; Pandey, N. K. Electrolytic and ozone aided destruction of oxalate ions in plutonium oxalate supernatant of the PUREX process: A comparative study. *J. Radioanal. Nucl. Chem.* **2021**, *328* (3), 857−867.

(5) Sun, J.; Lu, H.; Lin, H.; Du, L.; Huang, W.; Li, H.; Cui, T. Electrochemical oxidation of aqueous phenol at low concentration using Ti/BDD electrode. *Sep. Purif. Technol.* **2012**, *88*, 116−120.

(6) Roberts, J. G.; Voinov, M. A.; Schmidt, A. C.; Smirnova, T. I.; Sombers, L. A. The Hydroxyl Radical is a Critical Intermediate in the Voltammetric Detection of Hydrogen Peroxide. *J. Am. Chem. Soc.* **2016**, *138* (8), 2516−2519.

(7) Pei, S.; You, S.; Ma, J.; Chen, X.; Ren, N. Electron Spin Resonance Evidence for Electro-generated Hydroxyl Radicals. *Environ. Sci. Technol.* **2020**, *54* (20), 13333−13343.

(8) Jing, Y.; Chaplin, B. P. Mechanistic study of the validity of using hydroxyl radical probes to characterize electrochemical advanced oxidation processes. *Environ. Sci. Technol.* **2017**, *51* (4), 2355−2365.

(9) Leinisch, F.; Ranguelova, K.; Derose, E. F.; Jiang, J.; Mason, R. P. Evaluation of the Forrester-Hepburn mechanism as an artifact source in ESR spin-trapping. *Chem. Res. Toxicol.* **2011**, *24* (12), 2217−2226.

(10) Leinisch, F.; Jiang, J.; Derose, E. F.; Khramtsov, V. V.; Mason, R. P. Investigation of spin-trapping artifacts formed by the Forrester-Hepburn mechanism. *Free Radical Biol. Med.* **2013**, *65*, 1497−1505.

(11) Eberson, L.; Balinov, B.; Hagelin, G.; Dugstad, H.; Thomassen, T.; Forngren, B.; Forngren, T.; Hartvig, P.; Markides, K.; Yngve, U.; Ögren, M. Formation of Hydroxyl Spin Adducts via Nucleophilic Addition Oxidation to 5, 5-DimethyI-1-pyrroline N-Oxide. *Acta Chem. Scand.* **1999**, *53*, 584−593.

(12) Cerri, V.; Frejaville, C.; Vila, F.; Allouche, A.; Gronchi, G.; Tordo, P. Synthesis, redox behavior and spin-trap properties of 2, 6-di-tert-butylnitrosobenzene (DTBN). *J. Org. Chem.* **1989**, *54* (6), 1447−1450.

(13) Martínez-Huitle, C. A.; Ferro, S.; de Battisti, A. Electrochemical incineration of oxalic acid: Role of electrode material. *Electrochim. Acta* **2004**, *49* (22−23), 4027−4034.

(14) Panizza, M.; Michaud, P. A.; Cerisola, G.; Comninellis, C. Anodic oxidation of 2-naphthol at boron-doped diamond electrodes. *J. Electroanal. Chem.* **2001**, *507* (1), 206−214.

(15) Tissot, G. B.; Anglada, A.; Dimitriou-Christidis, P.; Rossi, L.; Arey, J. S.; Comninellis, C. Kinetic experiments of electrochemical oxidation of iohexol on BDD electrodes for wastewater treatment. *Electrochem. Commun.* **2012**, *23*, 48−51.

(16) Panizza, M.; Michaud, P. A.; Cerisola, G.; Comninellis, C. Electrochemical treatment of wastewaters containing organic pollutants on boron-doped diamond electrodes: Prediction of specific energy consumption and required electrode area. *Electrochem. Commun.* **2001**, *3* (7), 336−339.

(17) Ganiyu, S. O.; El-Din, M. G. Insight into in-situ radical and non-radical oxidative degradation of organic compounds in complex real matrix during electrooxidation with boron doped diamond electrode: A case study of oil sands process water treatment. *Appl. Catal., B* **2020**, *279*, 119366.

(18) Song, H.; Yan, L.; Jiang, J.; Ma, J.; Zhang, Z.; Zhang, J.; Liu, P.; Yang, T. Electrochemical activation of persulfates at BDD anode: Radical or nonradical oxidation. *Water Res.* **2018**, *128*, 393−401.

(19) Marselli, B.; Garcia-Gomez, J.; Michaud, P. A.; Rodrigo, M. A.; Comninellis, C. Electrogeneration of Hydroxyl Radicals on Boron-Doped Diamond Electrodes. *J. Electrochem. Soc.* **2003**, *150* (3), D79−D83.

(20) Pei, S.; Shen, C.; Zhang, C.; Ren, N.; You, S. Characterization of the Interfacial Joule Heating Effect in the Electrochemical Advanced Oxidation Process. *Environ. Sci. Technol.* **2019**, *53* (8), 4406−4415.

(21) Geng, R.; Zhao, G. H.; Liu, M. C.; Lei, Y. Z. In situ ESR Study of Hydroxyl Radical Generation on a Boron Doped Diamond Film Electrode Surface. *Acta Phys.-Chim. Sin.* **2010**, *26* (6), 1493−1498.

(22) Bilski, P.; Reszka, K.; Bilska, M.; Chignell, C. F. Oxidation of the Spin Trap 5,5-Dimethyl1-pyrroline N Oxide by Singlet Oxygen in Aqueous Solution. *J. Am. Chem. Soc.* **1996**, *118* (6), 1330−1338.

(23) Takayanagi, T.; Kimiya, H.; Ohyama, T. Formation of artifactual DMPO-OH spin adduct in acid solutions containing nitrite ions. *Free Radical Res.* **2017**, *51*, 739−748.

(24) Yoshimura, M.; Honda, K.; Uchikado, R.; Kondo, T.; Rao, T. N.; Tryk, D. A.; Fujishima, A.; Sakamoto, Y.; Yasui, K.; Masuda, H. Electrochemical characterization of nanoporous honeycomb diamond electrodes in non-aqueous electrolytes. *Diamond Relat. Mater.* **2001**, *10* (3−7), 620−626.

(25) Zhou, S.; Bu, L.; Yu, Y.; Zou, X.; Zhang, Y. A comparative study of microcystin-LR degradation by electrogenerated oxidants at BDD and MMO anodes. *Chemosphere* **2016**, *165*, 381−387.

NOTE ADDED AFTER ASAP PUBLICATION

Figure 11 was incomplete in the version that published December 3, 2024. This has been corrected and the revised version re-posted December 4, 2024.

https://doi.org/10.1021/acsomega.4c08628
ACS Omega 2024, 9, 49839−49848